CHEMISTRY
A EUROPEAN JOURNAL

Towards a Better Understanding of Magnetic Interactions within *m*-Phenylene α-Nitronyl Nitroxide and Imino Nitroxide Based Radicals, Part III: Magnetic Exchange in a Series of Triradicals and Tetraradicals Based on the Phenyl Acetylene and Biphenyl Coupling Units

Laure Catala,[b] Jacques Le Moigne,[c] Nathalie Gruber,[a] Juan J. Novoa,[d] Pierre Rabu,[c] Elie Belorizky,[e] and Philippe Turek*[a]

Abstract: The present work completes and extends our previous reports[1,2] on the determination of the magnetic ground state and on the strength of the through bond exchange coupling within series of biradicals. This knowledge was subsequently exploited for the analysis of the magnetic interactions in their crystals. We report here the studies of series of triradicals incorporating α-nitronyl nitroxides (**NN**) or α-imino nitroxides (**IN**) as terminal radical fragments connected through a *m*-phenylene coupling unit in one case and a phenyl acetylene unit in other case. Tetraradical derivatives have also been studied. The studies of isolated molecules (EPR in solution and DFT calculations) allow the assessment of the magnetic interactions through the magnetic coupling unit. All triradical derivatives are found to exhibit a quartet ground state, whereas a singlet ground state is determined for the tetraradical. This last result reinforces previous findings that the singlet ground state is favoured in related biradicals involving similar *m*-phenylene couplers. Moreover, the through bond magnetic exchange coupling for the *ortho–meta* connectivity could be demonstrated as being ferromagnetic, thus ascertaining our previous hypotheses.[1] The magnetic properties of the triradicals and tetraradicals in their solid state have been rationalized by using a previously proposed methodology,[2] allowing to identify the most relevant magnetic pathways.

Keywords: density functional theory · EPR spectroscopy · magnetic properties · molecular materials · radicals

[a] Dr. N. Gruber, Prof. P. Turek
Institut Charles Sadron (CNRS-UPR 22)
Université Louis Pasteur, 6 rue Boussingault
67083 Strasbourg (France)
Fax: (+33) 388-414-099
E-mail: turek@ics.u-strasbg.fr

[b] Dr. L. Catala
Institut de Chimie Moléculaire et des Matériaux d'Orsay
bâtiment 420, Université Paris-Sud
91120 Orsay (France)

[c] Dr. J. Le Moigne, Dr. P. Rabu
Institut de Physique et Chimie des Matériaux
de Strasbourg (CNRS-UMR 7504), Université Louis Pasteur
23 rue du Loess
67034 Strasbourg (France)

[d] Prof. J. J. Novoa
Departament de Química Física
Facultat de Química and CERQT, Park Cientific
Universitat de Barcelona, Av. Diagonal 647
08028 Barcelona (Spain)
Associate Member of the CEPBA-IBM Research Institute

[e] Prof. E. Belorizky
Laboratoire de Spectrométrie Physique (CNRS-UMR 5588)
Université Joseph Fourier, B. P. 87
38402 Saint Martin d'Hères Cedex (France)

Supporting information for this article is available on the WWW under http://www.chemeurj.org/ or from the author.

Introduction

Molecular-based magnetism is an active research area with respect to the promising new materials that might be prepared in the near future, whether at the macroscopic scale or at the so-called nanoscale.[3] Purely organic magnets are of special interest as they combine properties of organic materials, such as solubility and transparency, and offer the possibility of combining magnetic, optical, mechanical properties by the fine-tuning of organic synthesis.[4] Apart from the purely organic approach, such paramagnetic molecules are also good candidates for generating original networks by coordination with transition metal ions and reinforcing the magnetic interactions between them.[5] Two different strategies can be distinguished, namely the intramolecular ("through-bond") and the intermolecular ("through-space"). The intermolecular approach consists in using supramolecular engineering tools, for example, hydrogen bonds[6] to provide a better control of the packing of radical moieties, aiming at the generation of a 3D magnetic network to get magnetic order. However, there is still much to do to predict a priori the magnetic behaviour exhibited by a compound just looking at the molecular packing.[7] The intramolecular

DOI: 10.1002/chem.200400552

Abstract in French: *Le présent travail complète et étend nos travaux précédents portant sur la détermination des couplages d'échange magnétique intramoléculaires de séries de biradicaux,[1,2] et partant de cette connaissance, de l'analyse des corrélations magnétostructurales dans l'état cristallin. Nous présentons ici l'étude de séries de triradicaux comprenant des radicaux α-nitronyl nitroxydes (**NN**) ou α-imino nitroxydes (**IN**) substitués en* méta *d'un groupement phénylène d'une part, et en para d'un groupement phénylène éthynylène d'autre part. Des dérivés tétraradicalaires ont aussi été synthétisés et étudiés. Les interactions d'échange magnétique à travers les liaisons sont estimées d'après l'étude de ces molécules isolées par RPE en solution ainsi que par des calculs effectués dans l'approximation de la fonctionnelle densité (DFT). Alors que l'ensemble des dérivés triradicalaires présente un état fondamental magnétique quartet de spin, un état singulet est proposé pour les tétraradicaux. Ce dernier résultat confirme nos travaux précédents[1] ayant conclu à un état fondamental singulet pour des biradicaux basés sur le même coupleur. De plus, le couplage d'échange magnétique au travers du coupleur phénylène éthynylène pour des biradicaux substitués dans une topologie* ortho–méta *est ferromagnétique, confirmant ainsi les hypothèses antérieures.[1] Suivant une méthodologie précédemment décrite,[2] les propriétés magnétiques des triradicaux à l'état cristallin ont pu être analysées dans le détail et permettent de proposer des chemins d'interaction magnétique et des géométries de contacts intermoléculaires précises pour l'établissement d'interactions magnétiques bien identifiées.*

Abstract in Spanish: *El presente trabajo completa y extiende nuestras anteriores estudios[1,2] sobre la determinacion del estado fundamental magnético y la fuerza del intercambio magnetico a través del enlace en una serie de biradicales. Esta información es luego usada en el análisis de las interacciones magneticas dentro de sus cristales. En este trabajo presentamos los estudios sobre una serie de triradicales que contienen α-nitroxidos nitronílicos (**NN**) o α-imino nitróxidos (**IN**) como fragmentos radicalarios terminales conectados a través de unidades acopladoras del tipo* m*-phenilénicas, en un caso, y fenil acetilénicas, en el otro. Se han estudiado también tetraradicales. Los estudios con moleculas aisladas (EPR en disolución y DFT) permiten evaluar las interacciones magneticas a través de las unidades acopladoras. Todos los triradicales se ve que presentan un estado fundamental del tipo cuadruplete, mientras que el cuadruplete se cree que tienen un estado fundamental singlete. Este último resultado refuerza las conclusiones de un estudio previo en el que se vió que el singlete es el estado fundamental en biradicales similares conectados por una unidad* m*-fenilénica. Además, el intercambio magnético a través del enlace para la conectividad* orto *y* meta *se demuestra que es ferromagnetica, confirmando hipótesis anteriores.[1] Las propiedades magnéticas de los triradicales y tetraradicales en su estado sólido se han racionalizado empleando una matodología propuesta anteriormente,[2] identificando los caminos magnéticos relevantes.*

approach is based on the connection of radical fragments via a conjugated coupler, so as to provide high spin molecules by controlling the nature of the magnetic interactions of the spins.[8] Exploiting this way may result in the obtaining of magnetic organic polymers.[9] However, understanding intramolecular interactions in polymers is complicated by the presence of defects, and requires model compounds to assess precisely the strength and nature of the magnetic interactions through the conjugated coupler. To do so, it is of utmost importance to study oligoradicals based on various coupling units.

Following such guiding principles, some of our previous work (Part I)[1] considered biradical derivatives consisting of two imino-nitroxides (**IN**) radicals connected in a *meta* configuration through a phenyl acetylene coupler. A singlet magnetic ground state was found for the *meta* derivatives,[1] whereas the widely used "topological rules"[10] predicted a triplet ground state[11] as long as the torsion angle between the phenyl and the radicals remains small.[12] Since little was known for the *m*-phenylene bridging unit when connected to nitronyl nitroxides (**NN**) and imino nitroxides **IN**, we first investigated model biradicals and an extensive study has been previously reported (Part II).[2]

In the present work, we extend the previous results by designing triradicals and tetraradicals (Scheme 1). The work on triradicals is a direct extension of our previous work, both for the phenyl acetylene magnetic coupling unit (Part I) and for the *m*-phenylene bridging unit (Part II). The biphenyl bridge[13] has also been studied in order to investigate the effects on the intramolecular exchange coupling of a more distorted but shorter coupling unit. Furthermore, some hetero-triradicals were synthesized in order to assess the influence of the nature of the connected radicals, that is, **NN** versus **IN**. Not only such compounds permitted to study the variation of the strength of intramolecular magnetic interactions, but they also provided a nice way to understand the solid state magnetic behaviour within isostructural series. Following the procedure depicted in Part II, slight modifications of the geometry at the intermolecular contacts (structural motives) could be related to the variation of the magnetic behaviour. Indeed, statistical studies have shown

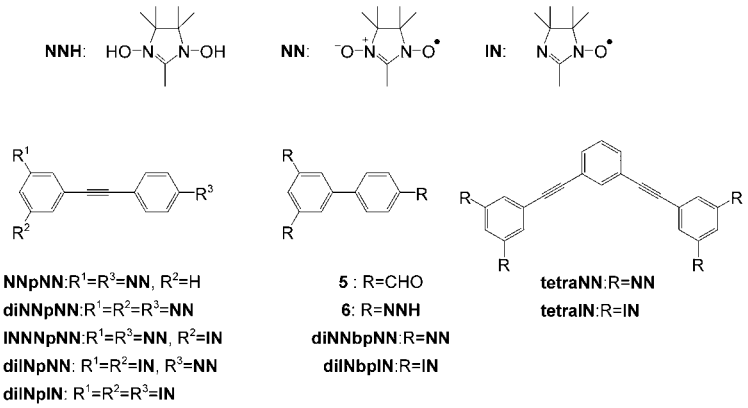

Scheme 1. Target radicals and some intermediates.

that considering the shortest contacts in the structure and applying McConnell's first principle failed to predict the predominant magnetism, and that comparing similar patterns could ensure reliable magneto-structural correlations.[7]

The overall ideas for the synthesis and for the study of the tetraradical derivatives was to investigate the possible effects of the change in the spin configuration in the *m*-phenylene based phenyl acetylene magnetic coupling unit reported in Part I. This is achieved by substitution of the **IN** terminal radical fragment studied in Part I with the triplet ground state *m*-phenylene based biradicals studied in Part II. We here report the synthesis of such oligoradicals, the assessment of their magnetic ground state by EPR study in dilute solution and by DFT calculations, as well as the magneto-structural correlations in the solid state.

Results and Discussion

Synthesis: The target compounds are presented on Scheme 1. The palladium-based synthesis of the phenyl acetylene based oligoradicals was complicated by side reactions such as dehydration from **NN** precursors to **IN** ones as well as homocoupling. Various synthetic routes (illustrated in Scheme 2 for a phenyl acetylene triradical) were explored for the triradical series to prevent such side reactions and have been shortly reported elsewhere.[14] Coupling the imidazolidine precursors (**NNH**) through route A ended up with side products, even if direct introduction of $[PdCl_2(PPh_3)_2]$ instead of in situ generation reduced the dehydration processes. However, this procedure leads to the isolation of the hetero-triradicals **INNNpNN** and **diINpNN**. The route consisting in coupling the paramagnetic building blocks (B), which was nicely used in some related pyridine compounds,[15] did not give any of the target compounds even when performed with other amines than triethylamine to fasten the reaction[16] (diisopropylamine, pyrrolidine), due to the fast decomposition of the radical fragments. Coupling the formyl precursors (C) followed by condensation of the bishydroxylamine with the formylated derivatives and final oxidation[17] was the best way to obtain compounds bearing **NN** fragments. Hence, the four phenyl acetylene based triradicals were obtained with the following yields: 49% for **diNNpNN** (overall yield through route C), 15% of **INNNpNN** (through via A), 22% for **diINpNN** triradical (selectively through route A) and 54% of **diINpIN** from reduction of **diNNpNN** by $NaNO_2$ in acidic media. The precursor of the biphenyl derivative **diNNbpNN** was obtained in high yield by using route C by Suzuki coupling[18] of the 5-bromoisophtalaldehyde to the *p*-formyl boronic acid in the presence of catalytic amount of tetrakistriphenyl phosphine palladium catalyst, followed by triscondensation with bishydroxylamine. Oxidation of the compound by sodium periodate in dichloromethane/water mixture afforded the desired triradical. Attempts to do the cross-coupling of the **NN** derivatives instead of the formylated ones did not succeed, since deboronation of the boronic acid occurred, as reported in other cases.[19] To obtain the tetraradicals, coupling 1,3-bis(1,3-hydroxy-4,4,5,5-tetramethylimidazolin-2-yl)-5-ethynylbenzene (Part II) to either dibromobenzene or diiobenzene in the presence of diisopropylamine and tetrakistriphenyl phosphine palladium was performed. The compound was precipitated and directly oxidised to give the tetraradical **tetraNN** with an overall yield of 9% when dibromobenzene was used and 17% with diiodobenzene. When the precipitated compound was dehydrated with 15% SeO_2 prior to MnO_2 oxidation,[20] **tetraIN** could be isolated in a 31% yield. The other pathway, using 1,3-diethynylbenzene and the brominated biradical precursor did not lead to the target tetraradicals, since degradation by homocoupling or polymerization side reactions of the 1,3-diethynylbenzene occurred. All compounds were characterized by elemental analysis and FAB spectrometry.

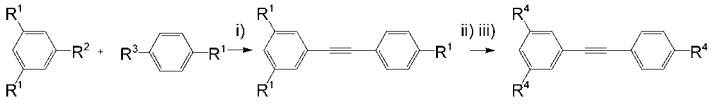

A: i) R^1=**NNH**, R^2=Br, R^3= CCH: $[PdCl_2(PPh_3)_2]$, CuI, triethylamine, 80°C, ii) R^4=**NN**, MnO_2, CH_2Cl_2

B: i) R^1=**NN**, R^2=Br, R^3= CCH: $[Pd(PPh_3)_4]$, amine/benzene

C: i) R^1=CHO, R^2=CCH, R^3= Br: $[Pd(PPh_3)_4]$/diisopropylamine/benzene, ii) R^4=**NNH**, bishydroxylamine, MeOH, Ar, iii) R^4=**NN**, MnO_2, CH_2Cl_2

Scheme 2. Synthetic routes A, B, C for obtaining **diNNpNN**.

Intramolecular magnetic exchange coupling: The EPR spectra of the oligoradicals were recorded in dilute (ca. 10^{-3}–10^{-4} mol) dichloromethane/acetone (1:1) solutions.

Triradicals: The **NN** substituted triradicals **diNNpNN** (Figure 1) and **diNNbpNN** showed the expected thirteen line spectrum corresponding to the strong exchange limit, that is, the exchange interaction between radical fragments *J* is much larger than the hyperfine coupling constant (hfcc).[21] The EPR spectra in fluid solution are well reproduced[22] with the parameters reported in Table 1. The spectrum of **diINpNN** could not be properly simulated. An asymmetry is observed, which is attributed to the superposition of conformations in strong and weak exchange, result-

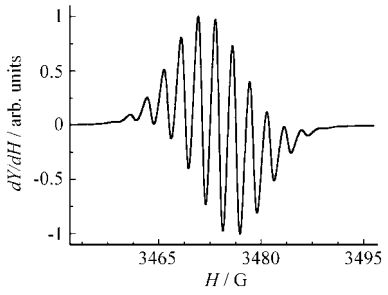

Figure 1. Room temperature EPR spectrum of triradical **diNNbpNN** in solution (CH_2Cl_2/acetone). The simulated spectrum matches perfectly the experimental spectrum.

Table 1. EPR parameters (^{14}N hfcc values for non-equivalent nuclei, g factor, line width, Gaussian/Lorentzian line shape ratio) used to simulate the EPR spectra of the various triradical derivatives in solution at room temperature.

Compound	a_{N1}[G]	a_{N2}[G]	a_{N3}[G]	g	ΔB/G	Gauss/Lorentz
diNNpNN	2.50	–	–	2.0067	1.8	100
diNNbpNN	2.50	–	–	2.0066	1.4	100
INNNpNN	2.50	3.10	1.42	2.0063	1.1	100
diINpIN	3.05	1.45	–	2.0059	1.4	50
diINbpIN	3.02	1.51	–	2.0060	1.4	80

ing in the triradical signal (strong exchange) superimposed with the biradical and monoradical species (weak exchange). These different species have slightly different g values, thus explaining the asymmetry of the spectrum. The superposition of contributions from monoradical and biradical is also required to improve the simulation of the EPR spectrum of **diINpIN**. Notably the overall appearance of the spectrum of for example **diINpNN** strongly depends on the used solvent, that is, aromaticity, polarity, bulkiness. This stresses the effects of molecular conformation on the exchange coupling, as recently evidenced in trimethylenemethane-based diradicals.[23] Actually, if the rotation barrier of the radical fragments with respect to the magnetic coupler is low enough in energy, the molecular conformation strongly depends on the molecular environment. In turn, the exchange coupling depends on the molecular conformation. Therefore, dynamical effects are expected in fluid solution, and the determination of the exchange coupling in a frozen solution should better be considered as a conformational average. It turns out that in Part II, we could estimate such average values in frozen solution as being close to the corresponding values in the crystalline state, that is, for one dominant conformation. This is also verified in the present work.

In frozen solutions, the characteristic spectrum of a quartet state exhibits five transitions, with a distance of $2D'_{Q4}$ (zero field splitting, ZFS parameter) between the two internal lines and $4D'_{Q4}$ between the two external ones.[24] The value of the D'_{Q4} can be related to the triplet ZFS parameter D'_T by the relation $D'_{Q4}=D'_T/3$, provided that the dipolar interaction between the biradical part and the monoradical can be neglected. Since the distance between those is quite long, this relation can be used for the present triradicals. We could thus compare the conformation of the biradical part to the biradicals previously studied in frozen solutions (Part II), so as to know whether we could expect the same magnetic exchange interaction through the m-phenylene fragment of these triradicals.

The frozen solutions were studied in a dichloromethane/acetone 1:1 mixture at a concentration of 10^{-3} M. The central line present on all spectra is due to the population of the doublet (Figure 2). A half-field "forbidden" $\Delta M_S=\pm 2$ transition is observed for all compounds. However, no $\Delta M_S=\pm 3$ transition could be observed. The experimental ZFS parameters are reported in Table 2 in magnetic field units (D',$E'=0$). As shown in Table 2, the conformation of the m-phenylene biradical fragment (**diNN** moiety) within

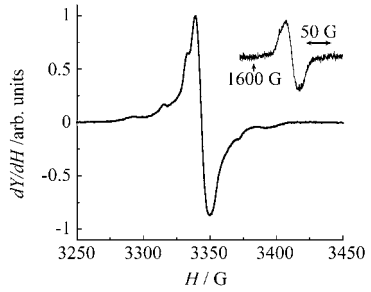

Figure 2. EPR spectrum of triradical **diINpNN** recorded in frozen solution (CH_2Cl_2/acetone) at $T=12$ K. In the inset is shown the half-field line ($\Delta M_S=\pm 2$) recorded with different spectrometer settings.

Table 2. Experimental ZFS splittings (D'_{Q4}) estimated in Gauss from the quartet lines of the EPR spectra of the triradical derivatives in frozen solution. The second column refers to the relation: $D'_{Q4}=D'_T/3$, and the last column (D^*_T) is given for the sake of comparison with the previous results obtained for the isolated m-phenylene based biradical fragments (Part II).[2]

	D'_{Q4}[G]	D'_T[G]	D^*_T[G][3]
diNNpNN	32±4	96±12	100–115
INNNpNN	18±1	54±3	67
diINpNN	26±2	78±4	90
diINpIN	26±2	78±4	90
diINbpIN	23± 2	69±6	90
diNNbpNN	39±4	117±12	100–115

diNNpNN and **diNNbpNN** is quite close to the related isolated biradicals; the D'_T value has been taken from Part II.[2] The other derivatives exhibit lower D'_T values as compared with the related isolated biradicals. This modification of the torsion of the radicals with respect to one another should thus affect the magnetic interactions through the m-phenylene magnetic coupling unit.

In the present work, the intramolecular exchange interaction has been assessed within some triradicals from the careful recording of the temperature dependence of the EPR susceptibility, that is, the doubly integrated EPR signal χ_{EPR}.[1,2,8e,25] The usual Curie plot (χ_{EPR} vs $1/T$) is linear for all compounds. It is well known[26] that the observation of the $\Delta M_S=\pm 2$ peak does not allow to conclude definitely to the quartet ground state against a triplet spin species. The forthcoming assessment of the quartet ground state is supported by i) the fit of the temperature dependence of the EPR susceptibility, which relevance is strengthened by the previous knowledge of the exchange coupling of the m-phenylene based biradical moiety (Part II), and ii) the results of computations performed at the DFT level for the molecular conformation found in the crystalline state. A consistency check is further given by the present studies of the magnetic properties of these triradicals in the solid state. In most cases, the temperature dependence of the peak-to-peak amplitude, A_{pp}, of the half-field signal is representative of the evolution of χ_{EPR} versus temperature, since no signal distortion is observed throughout the studied temperature range. A similar behaviour has been observed in the study

of the integrated EPR susceptibility for both the $\Delta M_S = \pm 2$ and the $\Delta M_S = \pm 1$ absorption lines, as shown on Figure 3. The $\chi_{EPR}T$ curves were normalised at high temperature to 1.125 emu K mol^{-1}, which is the value expected for three non interacting spins $S = {}^1/_2$.

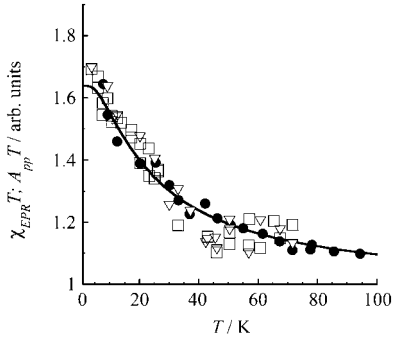

Figure 3. Temperature dependence of the χT product of the $\Delta M_S = 1$ (●) and $\Delta M_S = 2$ (▽) EPR lines together with the product of the peak-to-peak amplitude by temperature of the $\Delta M_S = 2$ (□) for the triradical **diNNpNN**. The full line is the fit of the data to Equation (1).

The data are fitted to the model depicted in Scheme 3. Three interacting $S = {}^1/_2$ spins are distributed at the apexes of an isosceles triangle (Scheme 4) with two different interactions J_1 and J_2 assuming that the g factor of each spin is equal to the free electron value, this model yields the following temperature dependence of the χT product [Eq. (1)]:[27]

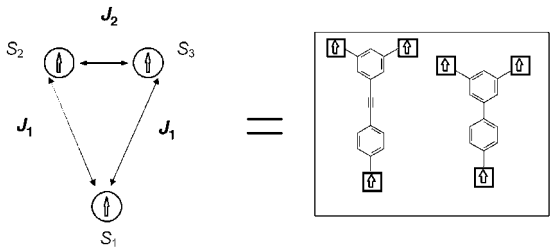

$$\hat{H} = -J_1\left(\hat{S}_1 \bullet \hat{S}_2 + \hat{S}_1 \bullet \hat{S}_3\right) - J_2\,\hat{S}_2 \bullet \hat{S}_3$$

Scheme 3. Isosceles triangle model with the corresponding Hamiltonian used to model the magnetic behaviour of the studied triradicals.

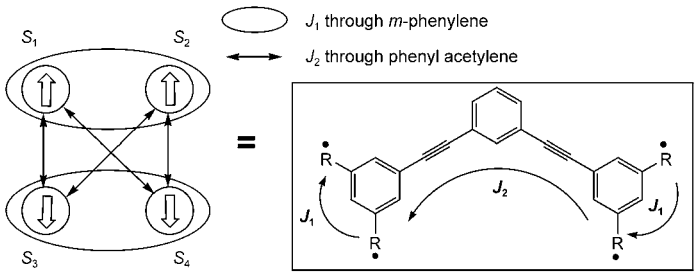

Scheme 4. Symmetrical four-spins system modelling the magnetic interactions within the studied tetraradicals.

$$\chi T = 0.375\left(\frac{10 + \exp(-\Delta_1/kT) + \exp(-\Delta_2/kT)}{2 + \exp(-\Delta_1/kT) + \exp(-\Delta_2/kT)}\right) \quad (1)$$

with $\Delta_1 = 3J_1/2$ and $\Delta_2 = (J_1 + 2J_2)/2$.

The homo-triradical **diINbpIN** could not be studied because of the weakness of the half-field transition. The results of the fits to Equation (1) for the EPR data of all compounds are summarized in Table 3. First of all, the quartet is found being the ground state for all studied triradicals. Hence, a ferromagnetic exchange interaction is effective through the *m*-phenylene unit and the phenyl acetylene or biphenyl unit between the present **IN**/**NN** radical fragments. It has to be pointed out that the magnitude found within the biradical part is in full agreement with those found in the biradical series (Part II), thus showing that EPR is a powerful experimental tool as long as careful studies are performed on dedicated series of compounds. Within the phenyl acetylene derivatives, the nature of the radical (**NN** or **IN**) on the biradical fragment has a direct influence on the magnitude of the exchange, as previously demonstrated in the biradical series. It is worth noting that a similar rule is found for triradicals, that is, a **NN** fragment connected *para* to the biradical part leads to a better delocalisation of the spin density on the phenyl acetylene coupler (cf. J_1/k) compared with an **IN** fragment. Moreover, the idea that connecting a triplet entity may modify the magnetic interaction through the phenyl acetylene coupler is demonstrated here, since the magnetic exchange is greater through the phenyl acetylene for the **diNNpNN** triradical than for the reported biradical **NNpNN** (Part I).[1] The modification is quite small, but still corroborates some results found on more robust triplet entities. Moreover, the ferromagnetic coupling is definitely proven experimentally for **NN** or **IN** radical fragments substituted in the 1,3- or 1,5-positions, that is, in the *para*–*meta* position, on a phenylene–ethynylene magnetic coupling unit. This could not be assessed experimentally in Part I.[1]

To have an independent indication that the quadruplet is the ground state in all these triradicals we carried out B3LYP/3-21G(d) calculations at their crystal geometry depicted in the section devoted to the solid-state properties. Some of the methyl groups are disordered in these crystals. In this case, we took for our calculations the option in which the methyl groups are closer to an alternated arrangement, with the C–C distance equal to the average one for the other methyl groups and the C–H distance equal to 1.1 Å. At this geometry, we computed the energy for the quadruplet and doublet states, imposing tight accuracy in the computation of the integrals and in the convergence of the self-consistent process. The results for all radicals show that the quadruplet is the ground state in all cases. The experimental and the calculated quadruplet-doublet splitting (Δ_2) are given in Table 4. The given results are for the doublet spin being localized in the radical fragment being connected to the singly substituted phenyl ring. Although two more doublet spin configurations may be considered, this spin distribution yields the lowest energy. A good agreement is found

Table 3. Values of the exchange coupling (expressed in K) through the *m*-phenylene magnetic coupling unit (J_2/k), and through the phenyl acetylene or the biphenyl magnetic coupling unit (J_1/k) deduced from the fits of the EPR data to Equation (1). The last row gives previous data (Part II) obtained for the isolated *m*-phenylene based biradicals, to be compared with J_2.

Exchange coupling	**diNNpNN**	**diNNbpNN**	**INNNpNN**	**diINpIN**	**diINpNN**
J_1/k [K]	7 ± 2	7 ± 2	$+7\pm2$	0.7 ± 0.1	1.0 ± 0.5
J_2/k [K]	23 ± 4	10 ± 7	15 ± 1	6.5 ± 1	$+6.5\pm4$
$J_{biradical}/k$ [K][2]	20–40	20–40	13–25	5–15	5–15

Table 4. Experimental and calculated quadruplet–doublet splitting (in K) for the studied triradicals.

Q–D splitting; Δ_2/K	**diNNpNN**	**diNNbpNN**	**diINpIN**	**diINpNN**	**INNNpNN**
experiment	27	14	7	7	19
theory	67	139	16[a]	8	40

[a] the unknown geometry has been chosen similar to the geometry of **diINpIN**, as suggested by the EPR results in frozen solution.

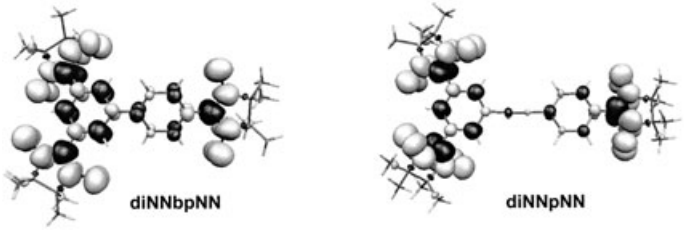

Figure 4. Spin density computed for some of the indicated triradicals at the UB3LYP/3-21G(d) level. The surfaces plotted are those of 0.002 atomic units of electronic density (positive in white, negative in black). The maximum of spin density is, in all cases, located in the NCNO or ONCNO five-membered ring group of atoms.

between theory and experiment when the *m*-phenylene biradical moiety of the triradicals is **diIN**, as previously observed for the singlet-triplet splitting of the isolated biradical (Part II). When dealing with **diNN** as the *m*-phenylene biradical moiety of the triradicals, the theoretical values are quite overestimated as already found in the corresponding isolated biradical (Part II). It has to be noticed the largest quadruplet–doublet found theoretically for the biphenyl magneto-coupler in **diNNbpNN**, whereas the experimental results point to a similar efficiency than the phenylene–ethynylene magnetic coupling unit. Indeed, the synthesis and the study of **diNNbpNN** were motivated by the idea that the biphenyl magnetic coupling unit may be more efficient than the phenylene–ethynylene one. However, neither the "thought experiment" nor the theoretical predictions could lead to the proper conclusion. Both the **diNNpNN** and **diNNbpNN** radicals present values well above the other triradicals (46.7 and 96.7 cm^{-1} vs. 5.7, 27.6 and 11.17 cm^{-1}). It is possible that the density functional methodology computed doublet–quadruplet energy differences are not completely reproduced, though previous estimates with other compounds indicate that these differences are within 10% of the experimental result. We expect that in this family of compound, whose structure is quite similar, the errors to be also constant. Thus, even if some error could exist, the trends between compounds are expected to remain. Therefore, these results suggest new molecular designs to induce stronger ferromagnetic interactions (the use of the **diNNpNN** and **diNNbpNN** radicals). We have not analyzed yet the reasons behind their stronger ferromagnetic interactions, but a first look indicates that are complex.

According to previous studies on nitronyl nitroxides and imino nitroxides, the quadruplet presents an electronic structure where the spin is located essentially over the ONCNO and ONCN atoms of the five-membered ring, being negative in the central C(sp^2) atoms and negative over the remaining atoms (see Figure 4). The six-membered ring presents sign alternation in all centers, being the largest atomic spin population (computed using the Mulliken analysis) 0.06 atomic units (au). The central C–C bond connecting the two six-membered rings in the **XpX′** radicals preserve the sign alternation (one has a spin population of 0.03 au and the other −0.03 au). It is also worth noting that the spin alternation is preserved in these radicals despite the lack of planarity between the two six-membered rings, and also between the five- and six-membered rings.

The influence of the conformation of the coupling unit may be considered by comparing the through magnetic coupling unit intramolecular interactions in the **diNNpNN** and the **diNNbpNN** triradicals. The phenyl rings in the phenyl–acetylene magnetic coupling unit in **diNNpNN** are twisted by 13°, whereas the biphenyl magnetic coupling unit in **diNNbpNN** is quite distorted with a dihedral angle of 36° between the phenyl rings. However, the exchange coupling J_2 is not much weakened through the biphenyl magnetic coupling unit compared with the phenyl acetylene one. Despite the longest through bond exchange pathway, the rigid and conjugated phenyl–acetylene bridge could be expected as being more efficient than a shorter but distorted one as is the biphenyl unit. Related to Part I of our work, this again points to the role of the sp hybridization through the acetylenic bond as a softener of the magnetic transmission.

Tetraradicals: In dilute solution, the EPR spectrum of **tetraNN** is expected to give 17 lines due to the hyperfine interaction of the unpaired electron with eight equivalent ^{14}N, whereas **tetraIN** should give 25 lines. However, the through-space dipolar interactions between the biradical fragments broaden the individual components of the hyperfine structure to result in a large envelope. Within such tetraradicals, we assume that the magnetic interactions are symmetrical with respect to the central phenyl ring (Scheme 4). Having noticed that the triplet species are not robust enough to consider that the triplet state is fully populated over the studied

temperature range, the following Hamiltonian yields the eigenstates of the four-spins system [Eq. (2)] depicted in Scheme 4:[27]

$$\hat{\boldsymbol{H}} = -J_1(\hat{\boldsymbol{S}}_1 \cdot \hat{\boldsymbol{S}}_2 + \hat{\boldsymbol{S}}_3 \cdot \hat{\boldsymbol{S}}_4) - J_2(\hat{\boldsymbol{S}}_1 \cdot \hat{\boldsymbol{S}}_4 + \hat{\boldsymbol{S}}_1 \cdot \hat{\boldsymbol{S}}_3 + \hat{\boldsymbol{S}}_2 \cdot \hat{\boldsymbol{S}}_3 + \hat{\boldsymbol{S}}_2 \cdot \hat{\boldsymbol{S}}_4) \quad (2)$$

The spin multiplicities are given as one quintet, Q5, three triplets, T_i, and two singlets, S_i. In frozen solution and for weakly coupled biradical fragments as it is the case here, the ZFS parameter for the quintet state, D'_{Q5}, can be related to each radical by the relation $D'_{Q5}=(D'_{T1}+D'_{T2})/6$.[8a] Both biradicals are equivalent, so that $D'_{Q5}=D'_T/3$ allows us to compare the conformations of the biradical fragments in the tetraradicals to the isolated biradicals as previously done for the triradical derivatives. The EPR spectra due to the $\Delta M_S=\pm1$ transition in frozen solutions can be due to the thermal population of the quintet and the triplets. The external lines from these states coincide so that the quintet state can be followed by its more internal lines. For the tetraradical **tetraNN**, the broadening prevents assignation of the lines, whereas some shoulders appear more distinctly in the **tetraIN** spectrum (Figure 5). The internal lines are separated

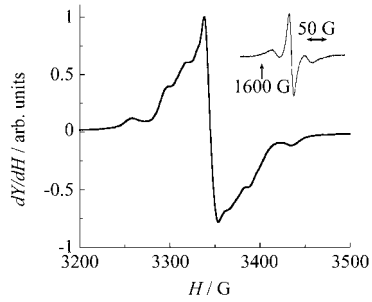

Figure 5. EPR spectrum of tetraradical **tetraIN** recorded at 4 K in frozen solution (CH_2Cl_2/acetone). In inset is shown the half-field line ($\Delta M_S=\pm2$) recorded with different spectrometer settings.

by 180 G which gives $D'_{Q5}=30\pm1$ G and $D'_T=90\pm3$ G. This value is found to be the same as for the corresponding *m*-phenylene based biradicals (see Table 2). Therefore, the strength of the exchange coupling is expected to be between 5 and 15 K as in the latter compounds. A peak corresponding to the $\Delta M_S=\pm2$ transition is detected for both tetraradicals, whereas the $\Delta M_S=\pm3$ and $\Delta M_S=\pm4$ lines could not be detected. As for the triradical derivatives, the knowledge of the S–T splitting of the biradical fragments together with the studies in the solid state will allow defining properly the magnetic ground state. However, two outer extra features with a lower intensity are observed on the side of the half-field line (Figure 5). This specific pattern has been observed for other species and can be considered to be characteristic of $S\geq2$.[28] The presence of this signal on the whole range of temperature ascertains the population of the quintet. The $\Delta M_S=\pm1$ and $\Delta M_S=\pm2$ transitions have been recorded in the 4–100 K range, but the $\Delta M_S=\pm1$ signal saturates over the whole range of temperature at all incident microwave power. Since the line shape does not change with temperature within this temperature range, the thermal behaviour of the EPR spin population involved in the half-field line is plotted as $A_{pp}T$ versus T on Figure 6. The decrease of $A_{pp}T$

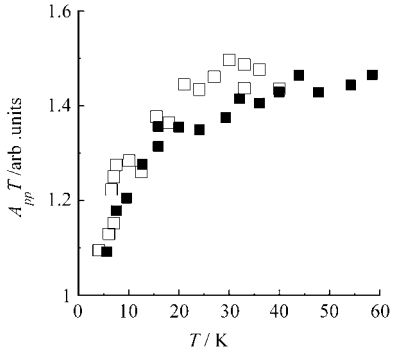

Figure 6. Temperature dependence of the product of the peak-to-peak amplitude of the EPR half-field line by the temperature for the tetraradicals **tetraIN** (■) and **tetraNN** (□) in frozen solution.

with the temperature means the depopulation of a high spin state to a lower spin state. The fitting by a four spin model is not relevant given the required large number of parameters for such a smooth variation. Numerous couples of (J_1, J_2) values yield a satisfactory correlation for the least squares fitting procedure. With respect to the previous results, modelling with a biradical interaction of +25 K and an antiferromagnetic interaction of −5 K through the phenyl acetylene coupler could reproduce the behaviour of **tetraNN**.

It can be qualitatively deduced from this study that the singlet is the ground state for both tetraradicals. This will be further discussed when considering the magnetic properties in the solid state. It is worth reminding that the singlet ground state has been found in related *m*-phenylene based phenyl acetylene biradicals (Part I). The present results confirm that the phenyl–acetylene magnetic coupling unit with this connectivity to **IN** or **NN** radicals does not obey the topological rules. It has to be pointed out that for stronger triplet species such as nitrenes, the same coupler gave ferromagnetic coupling.[29]

Solid-state properties: A convenient and widely used way to relate the magnetic properties to the molecular packing is to consider the signs of the spin densities involved in the shortest intermolecular contacts. The sign of the intermolecular exchange coupling is then attributed according to McConnell's first proposal.[30] The same sign of the spin densities at contact yields an antiferromagnetic coupling, whereas opposite signs would result in a ferromagnetic coupling. However, careful analysis have pointed out that the successful applications result from errors that compensate.[7] Nevertheless, we have reported in Part II that the study of a series of isostructural biradicals leads to a good analysis of the mag-

neto-structural properties. Indeed, the substitution of the **IN** radical by the **NN** radical slightly modifies a few contacts upon suppressing one oxygen atom. A way to simplify the analysis of a molecular packing within a crystal structure consists in determining the primary, secondary and tertiary patterns related to the strength of the hydrogen bonds in the structure. At intermolecular distances shorter than 5 Å, the contacts are considered between the molecular fragments known to bear the spin density, for example, between NO and any other atom. These are reviewed within each structure, considering the geometry of the contacts by using the QUEST program of the Cambridge Data Base for crystallographic data.[31] In the present study, such an analysis suggests a pathway for the intermolecular magnetic exchange. It results in a model for the description of the experimentally determined magnetic properties.

Phenyl–acetylene based triradical: The compounds **diNNpNN**, **INNNpNN** and **diINpNN** crystallised in the same space group $P2_1/n$ with very similar cell parameters (Table 5), as briefly reported in a previous communication.[14] A dichloromethane molecule is included in the unit cell, and the crystals remain solvated at room temperature. Compound **diINpIN** crystallises in the same space group but with different cell parameters, since there is no solvent molecule. In the case of **INNNpNN**, disorder is present on the internal oxygen atoms O_4 and O_6 (Figure 7). The three terminal radical fragments, that is, the five-membered rings, are numbered as cycle **1**, **2**, **3**. The oxygen atoms O_3 and O_5 (external positions) have a probability of presence of 90%, which is coherent with the external position solely observed in **diINpNN**. The internal oxygen atoms have a probability of presence of 60%. Hence, cycle **1** has an equal probability to be either a **NN** or **IN** fragment. Moreover, the **IN** cycle has only 10% probability to have the oxygen in an internal position. The dihedral angle between the phenyl rings and the planes of the ONCNO fragments is reported for the different compounds in Table 6.

In the following, we will focus on the series of isostructural compounds, hence discarding the **diINpIN** compound. Weak hydrogen bonds ($C(sp^3)$-H···O) and π–π stacking at 3.6 Å between the aromatic cycles generates head-to-tail dimers of triradicals related by an inversion centre. Two types of short contacts between the ONCNO fragments are found within these dimers (Table 7). The proximity of oxygen O_4 (cycle **1** of molecule 1) and cycle **3** of molecule **2** generates contacts gathered in group **1**. Three contacts are gathered in group **2**, which involves short contacts between NO fragments terminated by O_1 and O_5 and belonging to neighbouring molecules. As there is no occupied O_4 position in **diINpNN**, only contacts of group **2** are found for this compound. For **diNNpNN** and **INNNpNN**, the shortest contact in group **1** is found at 3.16 Å between the central carbon C_8 from cycle **3** (monoradical fragment) and the oxygen O_4 of cycle **1**. For **INNNpNN**, this short contact is present in only 55% of the cases, since O_4 site is not always occupied. No contact at a distance shorter than 4.5 Å is observed between the described dimers of triradicals, so that they can be considered as almost isolated with respect to magnetic pathways. The interatomic distances measured for the various contacts within different groups are reported in Table 7. The magnetic behaviour of the four synthesized derivatives is reported in Figure 8. As expected for such triradicals, the χT

Table 5. X-ray crystal structure and lattice parameters of the phenyl acetylene based triradical derivatives.

	diINpNN	**INNNpNN**	**diNNpNN**	**diNNbpNN**
formula	$C_{35}H_{43}N_6O_4 \cdot CH_2Cl_2$	$C_{35}H_{43}N_6O_5 \cdot CH_2Cl_2$	$C_{35}H_{43}N_6O_6 \cdot CH_2Cl_2$	$C_{33}H_{43}N_6O_6$
F_w	696.70	712.70	728.70	619.75
crystal system	monoclinic	monoclinic	monoclinic	triclinic
space group	$P2_1/n$	$P2_1/n$	$P2_1/n$	$P\bar{1}$
a [Å]	12.414(2)	12.297(1)	12.2541(7)	9.7410(2)
b [Å]	18.2021(9)	18.283(2)	18.293(2)	12.3790(5)
c [Å]	16.643(1)	16.796(2)	16.892(2)	15.3730(7)
β [°]	93.712(8)	93.88(2)	93.877(7)	104.567(1)
V [Å^3]	3752.8(9)	3767(1)	3777.9(1)	2635.1(3)
Z	4	4	4	2
ρ [g cm^{-3}]	1.23	1.26	1.28	1.27
data collected	5505	5794	6945	9119
data used for refinement $I>3\sigma(I)$	2935	2370	2451	4701
$R(I)$	0.084	0.058	0.061	0.046
$R_\omega(I)$	0.094	0.083	0.083	0.066

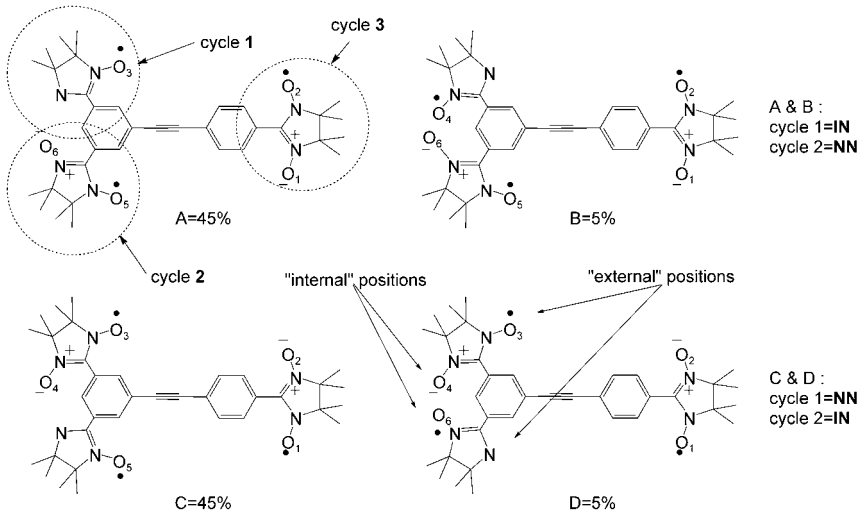

Figure 7. The four possible representations of the **INNNpNN** molecule with respect to the disorder: A, B, C, D give the corresponding probability as deduced from the XRD analysis.

Table 6. Dihedral angles formed by the radical cycles (numbering scheme defined in Figure 7) and the nearest phenyl ring within the four different triradical derivatives.

Compound	Cycle 1 [°]	Cycle 2 [°]	Cycle 3 [°]
diNNpNN	46	26	18
INNNpNN	43	25	17
diINpNN	37	22	15
diINpIN	21	3	17

Table 7. Summary of the shortest interatomic distances (intermolecular contacts, in Å) found between the ONCNO fragments within dimers of triradicals. Bold figures point to the shortest contacts.

Contacts	Group	**diNNpNN**	**INNNpNN**	**diINpNN**
$O_5\cdots O_1$	2	3.68	3.69	3.84
$O_5\cdots N_2$	2	3.47	3.53	3.53
$O_5\cdots N_1$	2	3.80	3.83	**3.69**
$N_1\cdots O_4$	1	**3.30**	**3.29**	–
$N_2\cdots O_4$	1	3.46	3.42	–
$O_4\cdots O_1$	1	3.77	3.68	–
$O_4\cdots C_8$	1	**3.16**	**3.16**	–

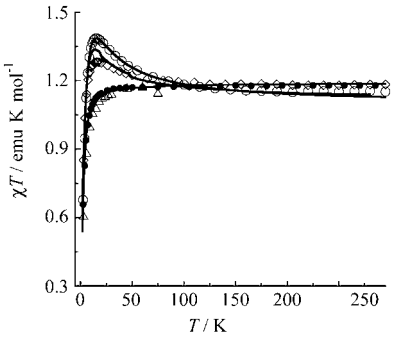

Figure 8. Temperature dependence of the static susceptibility (SQUID magnetometer measurements; applied magnetic field = 0.5 T) represented as the χT product for triradical derivatives: ● **diINpNN**; ○ **diNNpNN**; ◇ **INNNpNN** ; △ **diINpIN**. For the sake of clarity only 33% of the experimental data points have been plotted. Full lines represent the fits to the six-spins model depicted in Scheme 6.

product is close to 1.125 emu K mol^{-1} at room temperature. For **diINpIN** and **diINpNN**, the χT product remains unchanged as the temperature is lowered down to 10 K, whereas for **diNNpNN** and **INNNpNN**, a slight increase is observed to reach a maximum at 14.5 K of 1.39 and 1.28 emu K mol^{-1} respectively. This behaviour points out the presence of a ferromagnetic interaction within these molecular crystals. However, the further decrease at lower temperature indicates for all compounds that a neat antiferromagnetic intermolecular interaction dominates the magnetic properties in the low temperature regime.

The overall magnetic behaviour of **diINpIN** and **diINpNN** underlines weak magnetic interactions, as revealed by the flat Curie-like behaviour above 10 K. This is well understood when considering the intramolecular ferromagnetic couplings J_1 and J_2 for the isolated triradicals. A comparable or lower intermolecular antiferromagnetic interaction dominates the magnetic behaviour of these compounds at lower temperature.

Within the series of isostructural derivatives, the observed distinct behaviours may have two origins. The first modification of the magnetic exchange could be explained by the different contacts within the dimer of triradicals. Indeed, the presence of the ferromagnetic component in **INNNpNN** and **diNNpNN** can be related to group **2** of contacts, which is not involved in the structures of **diINpNN**. It has to be noticed that the short contact between a central carbon (C_8) bearing negative spin density and a nitroxide bearing positive spin density should result in a ferromagnetic interaction according to McConnell rules. However, in order to assign a given magnetic pathway, the detailed geometry of the contacts has to be considered and it should be compared with other similar compounds as previously discussed[7] and as demonstrated in Part II. To achieve this, we have chosen the biradical **diNNtmsa** (Scheme 5); its structure and magnetic

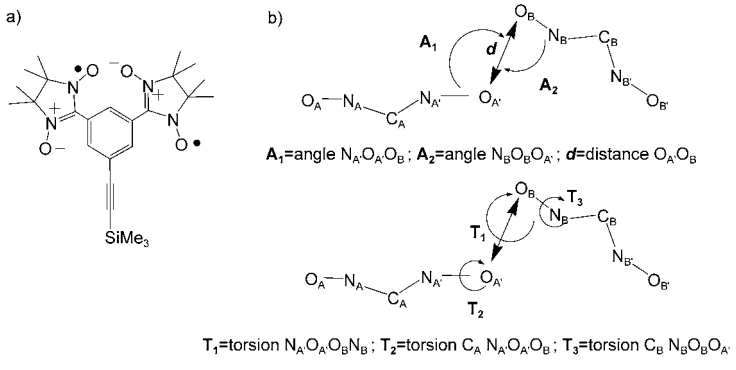

Scheme 5. a) Molecular scheme of the **diNNtmsa** biradical derivative. b) Definition of the geometrical parameters (distances, angles and torsions) for the description of the intermolecular contacts within dimers of **diNNpNN** and **diNNbpNN** compounds.

properties have already been reported in Part II.[2] This compound exhibits a similar pattern, which was found to generate unambiguously a ferromagnetic intermolecular interaction. The geometries are reported in Table 8 according to the definitions given in Scheme 5b. It appears that the geometries at these contacts are very similar, so that we can infer the existence of a ferromagnetic intermolecular pathway through these contacts observed within the dimers of triradicals in compounds **diNNpNN** and **INNNpNN**. Moreover, its magnitude could be close to 10 K as found in **diNNtmsa**. In a first approach, this may explain why the ferromagnetic trend is weaker in **INNNpNN** than in **diNNpNN**, since these contacts are altered by disorder in the former.

Not only the possible intermolecular magnetic interactions but also the intramolecular ones are different for the three compounds, as it has been demonstrated from the EPR studies of the triradicals in frozen solution (Table 3). It has been considered that the dihedral angle of the biradical fragment with respect to the phenylene ring is close to 30°.

Dihedral angles of 42 and 21° are found within the biradical fragment of **diNNpNN**. Therefore, a similar value of J_1 is expected for **diNNpNN** in frozen solution and in the solid state. The moderate torsion of cycle **3** (17°) should as well give a comparable value of J_2 in frozen solution and in the solid state. The simplest way to consider both intramolecular and intermolecular effects within the dimers of triradicals is given in Scheme 6 with a six-spins cluster with the parameters J_1 and J_2 as the intramolecular coupling constant, and J_3, J_4 as the intermolecular coupling constant related to group **1** and group **2**, respectively, previously defined types of contacts (see Table 7). Based on the previous results, some conditions may be fixed so as to reduce the number of parameters, hence improving the relevance of the fitting parameters. It is first noted that the previous measurements in the isolated state yield estimations of J_1 and J_2. Therefore, J_1 has been fixed between 0 and 40 K allowing the experimental data to be well adjusted for the **diINpNN** and **diNNpNN** (continuous lines in Figure 8) with the following sets of values in temperature units for **diNNpNN** $(J_1,J_2)=(+30.5\pm 3.1\text{ K},+12.3\pm 0.6\text{ K})$; $(J_3,J_4)=(+15.1\pm 0.9\text{ K},-17.7\pm 1.2\text{ K})$; and for **diINpNN** $(J_1,J_2)=(+2.0\pm 0.1\text{ K},+0.0\pm 0.02\text{ K})$; $(J_3,J_4)=(0\text{ K},-6.36\pm 0.03\text{ K})$. For these simulations, the g factor has been set to the free electron value. The set of values refined for the intramolecular exchange coupling is in good agreement with that found in the isolated state. For **INNNpNN**, a rough agreement is found upon setting (J_1,J_2) to the values found in the isolated state, that is, $(J_1,J_2)=(+15\text{ K},+7\text{ K})$. This procedure yields $(J_3,J_4)=(+12\text{ K},-14\text{ K})$, thus ascertaining the observed behaviour of **diNNpNN** and of **diINpNN**. It is worth noticing that the present set of (J_3,J_4) for **INNNpNN** does represent an average value for two sets, with and without J_3, with respective weight 55 and 45% as deduced from the analysis of the molecular packing. Along this line, and although being quite fortuitous, it may be noted the almost perfect overlap of the weighted sum (45/55) of the experimental susceptibility data of **diINpNN** and **diINpNN** with the data of **INNNpNN**. As concluded in the analysis of the crystal structure, the group **1** contacts results in a ferromagnetic interaction depicted by J_3 in **diNNpNN** and in **INNNpNN**. Its magnitude is in agreement with the value found for similar contacts in **diNNtmsa** (~10 K). As expected, J_4 is antiferromagnetic for all compounds. However, a value of 17 K is probably too high to be solely ascribed to the small difference of geometry between **diINpNN** and **diNNpNN**. This approach is certainly still oversimplified, but is interestingly consistent with both previous magneto-structural correlations and the intramolecular exchange coupling found through studies in the isolated state.

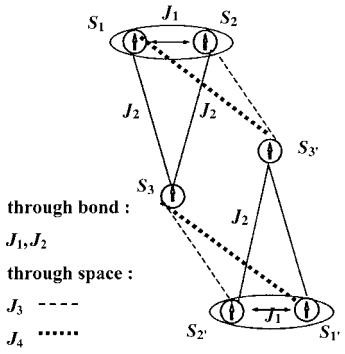

$$\hat{H} = -J_1\left(\hat{S}_1\cdot\hat{S}_2 + \hat{S}_{1'}\cdot\hat{S}_{2'}\right) - J_2\left(\hat{S}_1\cdot\hat{S}_3 + \hat{S}_2\cdot\hat{S}_3 + \hat{S}_{1'}\cdot\hat{S}_{3'} + \hat{S}_{2'}\cdot\hat{S}_{3'}\right)$$
$$- J_3\left(\hat{S}_{3'}\cdot\hat{S}_2 + \hat{S}_{2'}\cdot\hat{S}_3\right) - J_4\left(\hat{S}_1\cdot\hat{S}_{3'} + \hat{S}_{1'}\cdot\hat{S}_3\right)$$

Scheme 6. The six-spins system and its model Hamiltonian used for the simulation of the behaviour of the head-to-tail stacked dimers of triradicals formed in the solid state of **diINpNN** and **diNNpNN**.

Triradicals based on the biphenyl coupling unit: Single crystals were obtained only for **diNNbpNN** and the crystal structure could be refined, leading to the following parameters: triclinic space group $P\bar{1}$; with lattice parameters: $a=9.741$, $b=12.379$, $c=15.373$ Å, $\alpha=104.567$, $\beta=98.477$, $\gamma=110.690°$, $Z=2$. No disorder is observed for the asymmetric unit (see Supporting Information), and the torsion angles between the imidazolidine and the phenyl rings range between 10 and 22°. Short contacts C(sp^3)-H···O and C(sp^3)···N lead to a primary structure, which is made of dimers (molecules A and A′ in Figures S16 and S17) further connected to build up chains. Within the dimers, some short contacts are present between ONCNO fragments, due to the proximity of N_3O_3 groups: two contacts $O_3\cdots O_5$ at 3.75 Å and $O_3\cdots O_6$ at 4.02 Å, two contacts at 3.30 Å ($O_3\cdots N_5$) and 3.50 Å ($O_3\cdots N_6$) and the shortest contact $O_3\cdots C_\alpha$ at 3.03 Å. Along the a axis, the proximity of N_4O_4 groups of two molecules belonging to two different dimers leads to a short contact of $O_4\cdots O_4$ at 3.85 Å between the dimers: this extends the primary structure into the chains (see Supporting Information). Further short contacts are not observed between these chains. As for the **diNNpNN** derivative, a comparison of the geometry of the dimer within the two derivatives **diNNtmsa** and **diNNbpNN** shows that these molecular packings have similar geometries at contacts except for the O···O contact (Table 8).

The χT product reaches 1.11 and 1.03 emu K mol^{-1} at room temperature for **diNNbpNN** and **diINbpIN**, respectively (Figure 9). For **diINbpIN**, antiferromagnetic interactions dominate the overall behaviour down to 2 K. For

Table 8. Comparsion of the detailed geometries as depicted in Scheme 5 for two similar intermolecular contacts within **diNNpNN**, **diNNtmsa**[2] and **diNNbpNN**. C_α reads for C_A or C_B in the $ONC_\alpha NO$ ring of Scheme 5.

Contact	**diNNpNN** d[Å] (A_1,A_2,T_1,T_2,T_3)[°]	**diNNtmsa**[2] d[Å] (A_1,A_2,T_1,T_2,T_3)[°]	**diNNbpNN** d[Å] (A_1,A_2,T_1,T_2,T_3)[°]
$C_\alpha\cdots O$	3.16 (123, 94, 84, 83, 85)	3.03 (138, 98, 89, 85, 73)	3.03 (125, 96, 83, 85, 75)
O···O	3.77 (140, 62, 82, 88, 62)	3.70 (156, 62, 78, 77, 55)	3.75 (100, 60, 41, 65, 57)

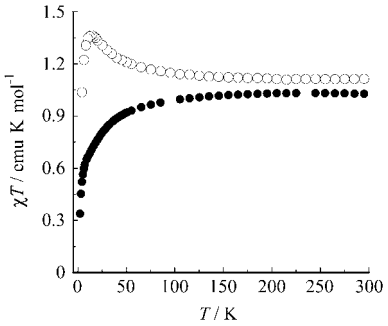

Figure 9. Temperature dependence of the static susceptibility (SQUID magnetometer measurements; applied magnetic field = 0.5 T) represented as the χT product for triradical derivatives: ● **diNNbpNN**; ○ **diINbpIN**.

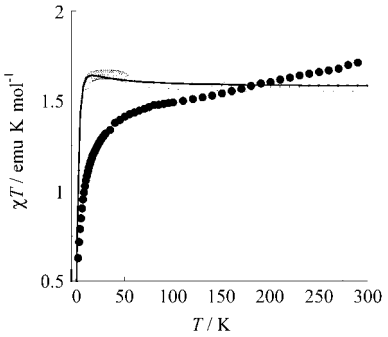

Figure 10. Temperature dependence of the static susceptibility (SQUID magnetometer measurements; applied magnetic field = 0.5 T) represented as the χT product for tetraradical derivatives: ● **tetraNN**; ○ **tetraIN**. The full line is the best fit to singlet-triplet equilibrium with a mean-field correction.

diNNbpNN, a maximum is observed by about 14 K with a value of 1.37 emu K mol^{-1}. Such a ferromagnetic interaction is attributed to the intramolecular magnetic exchange as expected from the results on the isolated triradicals. The decrease of χT at lower temperature indicates the competition with intermolecular antiferromagnetic interactions. The torsion angle between both rings of the biphenyl unit is quite large in the crystalline state, and we assume a J_2 coupling lower than 7 K as assessed in frozen solution. From an intermolecular point of view, the presence of a short contact between the central carbon and a nitroxide could again be responsible for some ferromagnetic interactions. The ferromagnetic component can thus be attributed to both intramolecular and intermolecular magnetic exchange. However, the six-spins cluster previously considered for almost isolated dimers of triradicals within **diNNpNN** and **diINpNN** does not yield a satisfactory fit of the data in the case of **diNNbpNN**. The interdimer interactions have to be considered, since short NO–NO contacts are observed between the biradical fragments of the triradicals as described before. Therefore, a proper but quite complicated model may be a chain of dimers of triradicals, which is not available to us. Moreover, the expected close values of the various acting interactions would strongly limit the relevance of such a complicated model, whenever available.

The magnetic behaviour of **diINbpIN** is not further considered, due to the lack of knowledge of both, the set of intramolecular exchange couplings (J_1,J_2) and the crystal structure determination. Nevertheless, there must be obviously a strong intermolecular antiferromagnetic interaction.

Tetraradicals: None of the attempts to obtain single crystals of the synthesized tetraradicals was successful. Therefore, the previous strategy for the analysis of the magneto-structural correlations is not applicable. The measurements of the magnetic properties performed in the solid state (Figure 10) will be used as a complementary analysis of the behaviour of the isolated molecule.

For both compounds, the value of χT is close to 1.5 emu K^{-1} mol^{-1} as expected with four independent $S = 1/2$ spins. Antiferromagnetic correlations are observed for both derivatives at low temperature. Whereas a continuous decrease is observed throughout the whole temperature range for **tetraIN**, a plateau with a slight increase is observed by about 20 K for **tetraNN**. Let us assume that such bulky molecules do pack without exhibiting short contacts so that the tetraradicals are quite isolated in the solid state. Then, the previously described four-spin model (Scheme 4) may be considered for the data fitting. Performing such a fit for **tetraNN** shows that neglecting the intermolecular interactions prevents a proper adjustment to the experimental data. The results of the fit give complementary indication of the intramolecular exchange couplings giving $J_1 = +12 \pm 1$ K, $J_2 = -2.5 \pm 0.1$ K. Similar results were obtained with the same model for the temperature dependence of the EPR signal of a small amount of polycrystalline powder of **tetraNN** leading to $J_1 = +14.1 \pm 0.3$ K, $J_2 = -2.0 \pm 0.1$ K. The best fit represented in Figure 10 is obtained with simple singlet–triplet equilibrium, that is, $J_2 = 0$ K, with a mean-field correction (Curie-Weiss temperature, θ) where $J_1 = +14$ K, and $\theta = -2$ K, but with a quite irrelevant Curie constant, $C = 2.1$ emu K mol^{-1}. It turns out that, although being not optimized, both of these approaches yield the proper range for the interaction J_1 within each biradical fragment, whereas the exchange coupling J_2 through the phenyl–acetylene magnetic coupling unit is suggested either vanishing or antiferromagnetic. However, the EPR studies in fluid solution have shown that the tetraradical does not consist in isolated biradical moieties. Moreover, it may be assumed a negative J_2, when referring to our previous report on J_2 being of the order -4 to -6 K (Part I).[1] Therefore, the present estimation of an antiferromagnetic J_2 corroborates the antiferromagnetic interaction through the *meta*-substituted phenyl–acetylene bridge, hence yielding the singlet ground state. This is unexpected, if one refers to the commonly accepted topological rules.[10] Furthermore, substituting a biradical fragment instead of a monoradical does not significantly change the through-bond exchange coupling. Worst-case, the qualitative trend is a weakening of J_2. The singlet ground state in these *m*-phenylene based di- and tetra-radical derivatives is not yet understood. Among possible ways, we may consider the non-robustness of the triplet state here

considered as compared to for example, nitrenes or carbenes. Another possible origin may be the spin polarization combined with the sp hybridization as mentioned when comparing the biphenyl magnetic coupling unit with the phenyl–acetylene.

Conclusion

The intramolecular exchange coupling between **IN** and/or **NN** radical substituents within triradical and tetraradical derivatives based on the *m*-phenylene moiety and linked by either a phenyl–acetylene or a biphenyl unit, has been properly assessed in the isolated state with the help of the EPR technique. The magnetic ground state of the triradicals has also been determined by DFT calculations. The main conclusions are: i) the quartet is the magnetic ground state for all triradicals and ii) the singlet state is very probably the ground state for all tetraradicals. Although being not yet fully understood, this violation of the so-called topological rules supports our previous findings (Part I)[1] that the phenyl–acetylene magnetic coupling unit in the *meta*-connectivity does not yield the high spin ground state. As discussed in Part II for the related biradical derivatives, the spin polarisation mechanism is presumably at the origin of the difference of magnetic coupling between **IN** or **NN** radical substituents. This tends to increase the spin density distribution over the coupling unit, hence increasing the through-bond magnetic exchange as exemplified for the *ortho–meta* connectivity ($J \sim 0$ K in **NNpNN** compared with $J = 7$ K in **diNNpNN**). The synthesis of isostructural compounds for series of triradicals afforded the possibility of a careful study based on a previously developed strategy (Part II). According to theoretical studies and statistical analyses, the relation between structure and magnetism requires considering the relative disposition of the whole molecules in the crystal.[7] This paper shows that the comparison of peculiar patterns is one objective way to deduce magnetic interaction pathways. The power and the relevance of this strategy are corroborated in the present work dealing with larger molecules bearing more magnetically active sites. In particular, the magnitude and the sign of most interactions were found similar in the solid state and in dilute solution, thus strengthening the validity of the various assessments performed by using either EPR in frozen solution or SQUID magnetometry. Comparing the peculiar patterns found in the contact geometries of basic building blocks, which individual magnetic properties have been properly assessed, is relevant for the comprehensive use of such complex molecules in a bottom-up approach of molecular magnetism.

Experimental Section

Materials and methods: Solvents were distilled under argon before use. In particular, THF was dried over sodium/benzophenone, triethylamine over KOH. All the reagents were used as received and purchased from ALDRICH. 4-bromoisophtaladehyde,[32] 5-ethynylbenzaldehyde, 1,3-bisformyl-5-ethynylbenzene[2] and 1,3-bis(1,3-hydroxy-4,4,5,5-tetramethylimidazolin-2-yl)-5-ethynylbenzene[2] were synthesised as reported elsewhere. 2,3-Bis(hydroxyamino)-2,3-dimethylbutane (bishydroxylamine) was synthesised using the procedure described in the literature.[33] Thin-layer chromatography (TLC) was performed on aluminium plates coated with Merck silica gel 60 F_{254}. Microanalyses were performed in the common facilities of the Institute Charles Sadron. Fast atom bombardment (FAB, positive mode) were recorded on a ZAG-HF-VG-Analytical apparatus in an *m*-nitrobenbyl alcohol (*m*NBA) matrix. ^{1}H and ^{13}C NMR spectra were recorded on a Bruker ARX 300 spectrometer. The EPR spectra have been recorded on X-band Bruker spectrometer (ESP-300-E) equipped with a rectangular TE 102 cavity. The static field was measured with an NMR Gaussmeter (Bruker ER 035) while the microwave frequency was simultaneously recorded with a frequency counter (HP-5350 B). Solutions were degassed by bubbling Argon directly in the EPR tube prior to measurements. The spin concentration has been estimated for all powder compounds by comparison with a standard sample (Varian pitch). It is reported hereafter as N_S (spin per molecule). Temperature was measured with a thermocouple (AuFe/Chromel) introduced inside the tube, at 1.5 cm from the bottom. As described in Part I[1] and Part II,[1] much care was devoted to the effects of microwave power saturation effects. At each temperature, the signal has been recorded at various power settings for the $\Delta M_S = 2$ line and for the $\Delta M_S = 1$ line. The various power levels were selected within different temperature range, depending on the limits for the observation of saturation effects. Magnetic susceptibility measurements were obtained with a Quantum Design MPMS/XL SQUID magnetometer.

CCDC-229617 (**diINpNN**), -229618 (**INNNpNN**), -229619 (**diNNpNN**) and -229727 (**diNNbpNN**) contain the supplementary crystallographic data for this paper. These data can be obtained free of charge from The Cambridge Crystallographic Data Centre via www.ccdc.cam.ac.uk/data_request/cif

Theoretical calculations: All calculations presented in this work were done with the B3LYP[34] non-local exchange-correlation density functional,[35] using the 3-21G(d) basis Gaussian basis set,[36] as implemented in the Gaussian 98 suite of programs.[37] The tight option was used to obtain enough accuracy in computing the integrals and energy.

***m*,*m*′-Bisformylbenzene 4-ethynyl benzaldehyde (1)**: 4-Ethynylbenzaldehyde (501 mg, 1.1 equiv) and $[Pd(PPh_3)_4]$ (292 mg, 8 % mol) were added under argon to 5-bromoisophtaldehyde (532 mg, 2.86 mmol). Benzene (25 mL) and diisopropylamine (8 mL) were added and the mixture was kept at 80 °C during 15 h. After the solution was cooled down, the ammonium salt was filtered, the filtrate was evaporated and the residue purified through chromatography on silica gel (CH_2Cl_2), to give a light yellow solid (556 mg, 74 %). M.p. 168 °C; ^{1}H NMR ([D$_6$]acetone): $\delta =$ 10.20 (s, 2H, CHO), 10.09 (s, 1H, CHO), 8.47 (t, 1H, Ph), 8.38 (d, 2H, Ph), 7.99 (d, 2H, Ph), 7.85 ppm (d, 2H, Ph); ^{13}C NMR ([D$_6$]acetone): $\delta =$ 192.3 (CHO),191.8 (CHO), 137.1, 135.9, 132.2, 129.6, 127.3, 123.5 (C-Ph), 90.6 (-C≡C-), 90.2 ppm (-C≡C-); IR (KBr): $\tilde{\nu} = 1693$ cm^{-1} (C=O); elemental analysis calcd (%) for $C_{17}H_{10}O_3$: C 77.86, H 3.84, N 18.30; found C 77.60, H 3.75, N 18.62.

***m*,*m*′-Bis(1,3-hydroxy-4,4,5,5-tetramethylimidazolin-2-yl)-4-ethynyl-1-(1,3-hydroxy-4,4,5,5-tetramethylimidazolin-2-yl)benzene (2)**: 2,3-Bis(hydroxyamino)-2,3-dimethyl butane (186 mg, 3.2 equiv) was added to a solution of trisaldehyde **1** (103 mg, 0.39 mmol) in MeOH (50 mL). A weak flow of argon was maintained during 3 d until the mixture was nearly dry. The white paste was filtered, washed with MeOH and dried to give a white solid (230 mg, 90 %). Elemental analysis calcd (%) for $C_{35}H_{52}O_6N_6$: C 64.39, H 8.03, N 12.87; found C 64.71, H 7.98, N 12.50; ^{1}H NMR ([D$_6$]acetone): $\delta = 7.67$ (m, 1H, Ph), 7.60 (m, 2H, Ph), 7.54 (d, $J = 9$ Hz, 2H, Ph), 7.46 (d, $J = 9$ Hz, 2H, Ph), 7.14 (s, 6H, OH), 4.71 (s, 3H, -HC imid.), 1.18 (s, 18H, CH_3), 1.10 ppm (s, 18H, CH_3); ^{13}C NMR ([D$_6$]DMSO): $\delta = 142.6$, 141.9, 130.9, 130.6, 129.9, 129.6, 128.7 (Ph), 92.1 (HC imid.), 89.9, 89.8 (C≡C), 66.2 (C_{quat} imid.), 24.4, 17.1 ppm (CH_3).

diNNpNN: Compound **2** (100 mg, 0.15 mmol) and MnO_2 (198 mg, 2.28 mmol, 5 equiv per radical) were added to a solution of CH_2Cl_2

(30 mL). The mixture turned dark blue and was stirred during 5 h, filtered and the solvent was evaporated. The residue was purified through chromatography (silica gel, AcOEt/CH_2Cl_2 1:9) to give **diNNpNN** (71 mg, 74%). Dark blue crystals containing one CH_2Cl_2 molecule per **diNNpNN** molecule could be grown by slow evaporation of a CH_2Cl_2/hexane mixture. M.p. 242°C (decomp); IR (KBr): $\tilde{\nu}=1363\ cm^{-1}$ (N–O); UV/Vis: $\lambda_{max}(\varepsilon)=319$ (53605), 371 (24680), 592 nm ($1130\ M^{-1}cm^{-1}$); elemental analysis calcd (%) for $C_{35}H_{19}O_6N_6{\cdot}CH_2Cl_2$: C 59.34, H 6.22, N 11.53; found C 59.11, H 6.20, N 11.28; MS FAB$^+$ (*m*NBA): *m*/*z*: 645.1 $[M+H]^+$, 629.1, 613.1, 597.1, 581.1, 565.1, 549.3, 533.1 (successive loss of 6 O), 514.0, 384.0 (successive loss of 2 fragments of 130 mass units); $N_S=3.1$ spins per molecule.

1,3-Bis(1,3-hydroxy-4,4,5,5-tetramethylimidazolin-2-yl)-5-bromobenzene (3): 5-Bromoisophtaladehyde (1.51 g, 7.05 mmol) and 2,3-bis(hydroxyamino)-2,3-dimethylbutane (2.42 g, 2.3 equiv) were added to MeOH (30 mL). The mixture was concentrated to almost dryness during 3 d. The white solid was washed with MeOH and dried, and a white powder was isolated (3.15 g, 94%). M.p. 175°C (decomp); IR (KBr): $\tilde{\nu}=3455\ cm^{-1}$ (OH); elemental analysis calcd (%) for $C_{20}H_{33}O_4N_4Br$: C 51.40, H 5.82, N 11.99; found C 51.27, H, 5.87, N 11.76; ^{1}H NMR ([D$_6$]DMSO): $\delta=7.81$ (s, 4H, -OH), 7.55 (s, 2H,Ph), 7.51 (s, 1H, Ph), 4.50 (s, 2H, -CH imid.), 1.07 (s, 12H, -CH_3), 1.03 ppm (s, 12H, -CH_3); ^{13}C NMR ([D$_6$]DMSO): $\delta=144$, 129, 128, 120 (C-Ph), 90 (CH imid.), 66 (C_{quat} imid.), 24 (CH_3), 17 ppm (CH_3).

1,3-Bis(1-oxyl-3-oxo-4,4,5,5-tetramethylimidazolin-2-yl)-5-bromobenzene (4): In a round-bottom flask containing a suspension of **3** (2.1 g, 4.44 mmol) in MeOH (100 mL), SeO_2 (74 mg, 6.65 mmol, 15% mol) was added.[20] After 2 d at room temperature, the yellow solution was evaporated and purified by chromatography (silica gel, CH_2Cl_2/EtOH 8:2) to give a yellow powder (1.65 g, 85%). ^{1}H NMR ([D$_6$]DMSO): $\delta=8.90$ (s, 1H, Ph), 8.30 (s, 2H, Ph), 1.36 (s, 12H, -CH_3), 1.30 ppm (s, 12H, -CH_3); ^{13}C NMR ([D$_6$]DMSO): $\delta=141$, 131, 129, 127 (Ph), 76 (CH imid.), 61.5 (C_{quat} imid.), 24 (CH_3), 19 (CH_3).

INNNpNN: In a round-bottom flask under argon, equipped with a funnel containing triethylamine (12 mL) distilled under argon, **3** (492 mg, 1.06 mmol), [$PdCl_2(PPh_3)_2$] (37 mg, 5% mol) and CuI (10 mg) were added. Triethylamine (7 mL) was added dropwise under stirring. 4-Ethynyl-(1,3-hydroxy-4,4,5,5-tetramethylimidazolin-2-yl)benzene (366 mg, 1.3 equiv) was dissolved in the remaining triethylamine (5 mL). This solution was added in five parts to the reaction mixture during 48 h, and heated to 80°C. After 12 h reaction time, partial dehydratation could be observed by TLC (silica gel, AcOEt/CH_2Cl_2 1:9). The mixture was cooled down, the amine salt filtered and the filtrate precipitated in hexane (200 mL). The precipitate (560 mg) was dried. Oxidation of this solid (270 mg) was performed by introducing MnO_2 (1.049 g, ~5 equiv per radical) in CH_2Cl_2 (25 mL). The suspension was stirred during 6 h at room temperature and turned to dark blue-green. The solution was evaporated and the remaining solid was purified by chromatography (silica gel, AcOEt/CH_2Cl_2 5:95) to isolate **diNNpNN** (37 mg) and **INNNpNN** (48 mg, 15%). Slow evaporation of a CH_2Cl_2/hexane mixture gave black needles of **INNNpNN**·CH_2Cl_2. M.p. 240°C (decomp); IR (KBr): $\tilde{\nu}=1365$ (N–O), 1549 cm^{-1} (C=N); UV/Vis: $\lambda_{max}(\varepsilon)=320$ (45250), 371 (16570), 450 (712), 595 nm ($700\ M^{-1}cm^{-1}$); elemental analysis calcd (%) for $C_{35}H_{19}O_5N_6{\cdot}CH_2Cl_2$: C 60.67, H 6.36, N 11.79; found C 60.55, H 6.39, N 11.65; MS FAB$^+$ (*m*NBA): *m*/*z*: 629.4 $[M+H]^+$, 613.4, 597.4, 581.4, 565.4, 549.3 (successive loss of 5 O), 514.4, 498.2, 384.1, 368.1; $N_S=2.8$ spins per molecule.

diINpNN: Compound **4** (400 mg, 0.91 mmol), [$PdCl_2(PPh_3)_2$] (30 mg, 5% mol) and CuI (5 mg, 3%) were dissolved in a solution of triethylamine (5 mL). A solution of 4-ethynyl-(1,3-hydroxy-4,4,5,5-tetramethylimidazolin-2-yl)benzene (277 mg, 1.2 equiv) in triethylamine (5 mL) was added to the funnel. This solution was added in portions of 1 mL during 48 h. The mixture was cooled down, the amine salt filtered and the filtrate precipitated in hexane. A yellow powder (220 mg) was isolated. ^{1}H NMR ([D$_6$]DMSO): $\delta=8.94$ (s, 1H, Ph), 7.93 (s, 2H, Ph), 7.83 (s, 2H, OH), 7.54 (m, 4H, Ph), 4.53 (s, 1H, -HC imid.), 1.11 (s,18H, CH_3), 1.04 ppm (s,18H, CH_3).

In a flask containing MeOH (30 mL), the yellow powder (105 mg) prepared above and MnO_2 (225 mg, ~5 equiv per radical) were introduced. After 5 h under stirring at room temperature and evaporation of the solvent, the residue was purified by chromatography (silica gel, AcOEt/CH_2Cl_2 5:95) and gave **diINpNN** (60 mg, 22% overall yield). Slow evaporation of a CH_2Cl_2/hexane mixture gave dark green crystals of **diINpNN**·CH_2Cl_2. M.p. 236°C (decomp); IR (KBr): $\tilde{\nu}=1363$ (N–O), 1544 cm^{-1} (C=N); UV/Vis: $\lambda_{max}(\varepsilon)=316$ (16370), 385 (62450), 445 (1380), 602 nm ($560\ M^{-1}cm^{-1}$); elemental analysis calcd (%) for $C_{35}H_{19}O_4N_6{\cdot}CH_2Cl_2$: C 62.06, H 6.51, N 12.06, O 9.18; found C 62.14, H 6.52, N 11.99, O 9.30; MS FAB$^+$ (*m*NBA): *m*/*z*: 613.2 $[M+H]^+$, 597.2, 580.2, 564.2, 548.2, (successive loss of 4 O), 498.1, 483.1, 384.0, 369.1, 353.1; $N_S=2.75$ spins per molecule.

diINpIN: Compound **diNNpNN** (45 mg, 0.069 mmol) and $NaNO_2$ (71 mg) were added to water/CH_2Cl_2 (1:1, 50 mL) acidified at pH 6. After 20 min, the bright red solution extracted with CH_2Cl_2, dried on Na_2SO_4 and evaporated. The red solid was purified by chromatography (silica gel, AcOEt/CH_2Cl_2 5:95) to give a red solid (25 mg, 59%). Crystals were grown by slow evaporation of a CH_2Cl_2/hexane mixture. M.p. 205°C (decomp); IR (KBr): $\tilde{\nu}=2208$ (C≡C), 1371 (N–O), 1543 cm^{-1} (C=N); UV/Vis: $\lambda_{max}(\varepsilon)=273$ (34450), 449 nm ($1441\ M^{-1}cm^{-1}$); elemental analysis calcd (%) for C 70.56, H 7.27, N 14.11; found C 70.32, H 7.26, N 14.04; MS FAB$^+$ (*m*NBA): *m*/*z*: 597.2 $[M+H]^+$, 581.1, 565.2, 549.2, (successive loss of 3 O), 483.2, 369.1 459.3, 345.1; $N_S=2.75$ spins per molecule.

***m*,*m*′-Bisformylphenyl-4-benzaldehyde (5)**: In a three-neck round-bottom flask containing triethylamine (50 mL), 5-bromoisophtalaldehyde (191 mg, 0.90 mmol) and 4-formylboronic acid (150 mg, 1.1 equiv) was added. A degassed aqueous solution (1.5 mL) containing Na_2CO_3 (212 mg, 2.2 equiv) was added with a syringe. Dimethoxyethane (5 mL) freshly distilled under argon were then added and the mixture was heated at 85°C. After 5 h of reaction, the reaction mixture was filtered and the filtrate was evaporated under vacuum. The residue was purified by chromatography (silica gel, AcOEt/CH_2Cl_2 1:99) to give a white solid (144 mg, 61%). M.p. 160°C (decomp); IR (KBr): $\tilde{\nu}=1691\ cm^{-1}$ (CHO); elemental analysis calcd (%) for $C_{15}H_{10}O_3$: C 75.62, H 4.23, N 20.15; found C 75.35, H 4.15, N 20.40; ^{1}H NMR ($CDCl_3$): $\delta=10.21$ (s, 2H, CHO), 10.12 (s, 1H, CHO), 8.42 (m, 3H, Ph), 8.05 (d, $J=8.5$ Hz, 2H, Ph), 7.86 ppm (d, $J=8.5$ Hz, 2H, Ph); ^{13}C NMR ($CDCl_3$): $\delta=191.5$ (CHO), 190.6 (CHO), 144.0, 136.3, 133.9, 131.7, 131.5, 127.9, 124.0 ppm (Ph).

***m*,*m*′-Bis(1,3-hydroxy-4,4,5,5-tetramethylimidazolin-2-yl)4-(1,3-hydroxy-4,4,5,5-tetramethylimidazolin-2-yl)benzene (6)**: The procedure was similar to the synthesis of **2**, using **5** (132 mg, 0.5 mmol) and 2,3-bis(hydroxyamino)-2,3-dimethyl butane (262 mg, 3.3 equiv) in distilled MeOH (30 mL) and CH_2Cl_2 (4 mL). After the usual workup, a white powder (294 mg, 85%) was isolated. M.p. 175°C (decomp); IR (KBr): $\nu=$ 3597 cm^{-1} (OH); ^{1}H NMR ([D$_6$]acetone): $\delta=7.72$ (s, 6H, OH), 7.63–7.55 (m, 7H, Ph), 4.59 (s, 3H, -HC_5), 1.09 (s,18H, CH_3), 1.06 ppm (s,18H, CH_3); ^{13}C NMR ([D$_6$]DMSO): $\delta=152.1$, 141.8, 140.8, 140.3, 139.2, 131.6, 128.9, 126.0 (Ph), 90.0 (HC imid.), 66.2 ($C_{quat.}$ imid.), 24.0, 16.9 ppm (CH_3).

diNNbpNN: The procedure used for obtaining **diNNpNN** was employed starting from **6** (103 mg, 0.16 mmol) and MnO_2 (198 mg, 2.28 mmol, 5 equiv per radical). The residue was purified by chromatography (silica gel, AcOEt/CH_2Cl_2 1:99) to give **diNNbpNN** (65 mg, 66%). M.p. 228°C (decomp); IR (KBr): $\tilde{\nu}=1360\ cm^{-1}$ (N–O); UV/Vis (CH_2Cl_2): $\lambda_{max}(\varepsilon)=$ 294 (43230), 371 (26420), 589 nm ($1380\ M^{-1}cm^{-1}$); elemental analysis calcd (%) for $C_{33}H_{19}O_6N_6$: C 63.95, H 6.99, N 13.57; found C 63.70, H 7.16, N 13.85; MS FAB$^+$ (*m*NBA): *m*/*z*: 621.2 $[M+H]^+$, 605.2, 589.2, 573.2, 557.2, 541.2, 525.2 (successive loss of 6 O), 490.1, 360.2; $N_S=3.2$ spins per molecule.

diINbpIN: Compound **diNNbpNN** (50 mg, 0.081 mmol) and $NaNO_2$ (168 mg, 10 equiv per radical) were added to a water/CH_2Cl_2 mixture (1:1, 50 mL) acidified at pH 6. After 20 min, the bright red solution extracted with CH_2Cl_2, dried on Na_2SO_4 and evaporated. The red solid was purified by chromatography (silica gel, AcOEt/CH_2Cl_2 5:95) to give a red solid (31 mg, 54%). Crystals were grown by slow evaporation of a CH_2Cl_2/hexane mixture. M.p. 245°C (decomp); IR (KBr): $\tilde{\nu}=1375\ cm^{-1}$

(N–O); UV/Vis (CH_2Cl_2): $\lambda_{max}(\varepsilon)=273$ (34450), 449 nm ($1441\,M^{-1}\,cm^{-1}$); elemental analysis calcd (%) for C 69.32, H 7.58, N 14.70; found C 69.43, H 7.54, N 14.39; MS FAB$^+$ (*m*NBA): *m*/*z*: 573.3 $[M+H]^+$, 557.3, 541.3, 525.3 (successive loss of 3 O), 459.3, 345.1; $N_S=3.3$ spins per molecule.

tetraNN: In a round-bottom flask, 1,3-diiodobenzene (150 mg, 0.45 mmol) and 1,3-bis(1,3-hydroxy-4,4,5,5-tetramethylimidazolin-2-yl)-5-ethynylbenzene (410 mg, 2.1 equiv), $[Pd(PPh_3)_4]$ (66 mg, 12 mol%) and freshly distilled diisopropylamine (10 mL) were added. The reaction mixture was heated at 80°C during 6 h. After filtration, evaporation of the filtrate, the concentrated solution was precipitated with pentane (100 mL). The beige powder was filtered and dried under vacuum (70% of estimated coupling).

The oxidation was performed on this powder dispersed in CH_2Cl_2 (100 mL). MnO_2 (382 mg, ~20 equiv) was added and the suspension was stirred at room temperature during 3 h. The mixture was worked up as usual and the residue purified by chromatography on a column and a second time on a preparative TLC support (silica gel, AcOEt/CH_2Cl_2/MeOH 19:80:1) to give a blue powder with an overall yield of 7% using the dibromobenzene, and 17% using diiodobenzene. IR (KBr): $\tilde{\nu}=1361\,cm^{-1}$ (N–O); elemental analysis calcd (%) for C 66.80, H 6.50, N 12.46; found C 66.56, H 6.76, N 12.50; UV/Vis (CH_2Cl_2): $\lambda_{max}(\varepsilon)=288$ (101210), 371 (63350), 585 nm ($2725\,M^{-1}\,cm^{-1}$); MS FAB$^+$ (*m*NBA): *m*/*z*: 899.3 $[M]^+$, 884.3, 868.3, 852.4, 836.4, 820.4, 804.3, 786.2, 770.2 (successive loss of 8 O), 769.2, 639.1, 509.3; $N_S=4.0$ spins per molecule.

tetraIN: The cross-coupling was performed as described for **tetraNN**, but after the reaction mixture was evaporated, the solid obtained (450 mg, 0.5 mmol) was treated with SeO_2 (10 mg, 15% mol) during 2 d in MeOH (200 mL). The suspension disappeared and the solution turned to yellow; the solvent was evaporated and the compound purified by chromatography (silica gel, CH_2Cl_2/EtOH 9:1 then gradually 6:4) to yield a yellow-brown powder (255 mg, 59%). ^1H NMR ([D$_6$]DMSO): $\delta=8.44$ (s, 2H, Ph), 8.22 (s, 4H, Ph), 7.80 (s, 1H, Ph), 7.66–7.63 (m, 3H, Ph), 1.16 (s,24H, CH_3), 1.14 ppm (s, 24H, CH_3).

To a suspension of this solid (200 mg, 0.22 mmol) in CH_2Cl_2 (30 mL), MnO_2 (380 mg, 4.4 mmol, 20 equiv) was added and the mixture stirred during 3 h. After filtration and evaporation of the filtrate the red compound was chromatographed (silica gel, AcOEt/CH_2Cl_2 15:85) to give **tetraIN** (110 mg, 31% overall yield) which gave solvated red needles unsuitable for structural determination by slow evaporation in a CH_2Cl_2/hexane mixture. M.p. 249°C (decomp); IR (KBr): $\tilde{\nu}=2216$ (C≡C), 1371 (N–O), 1549 cm^{-1} (C=N); UV/Vis (CH_2Cl_2): $\lambda_{max}(\varepsilon)=288$ (73390), 302 (62940), 447 nm ($1667\,M^{-1}\,cm^{-1}$); elemental analysis calcd (%) for **tetraIN**·3CH_2Cl_2: C 69.12, H 6.78, N 12.77, O 7.29; found C 68.91, H 6.82, N 12.56, O 7.84; MS FAB$^+$: *m*/*z*: 836.3 $[M+H]^+$, 821.3, 805.3, 789.3, 773.3 (successive loss of 4 O), 722.2, 608.1, 494.1; $N_S=4.1$ spins per molecule.

Acknowledgement

Dr. Marc Drillon (IPCMS, Strasbourg, France) is gratefully acknowledged for discussions of the model Hamiltonians of various spin clusters. Mr. Maxime Bernard (ICS, Strasbourg, France) is thanked for invaluable help in the set up of EPR experiments. J.J.N. acknowledges the support of CESCA/CEBPA in allocating computer times in their machines and also the financial support of the Spanish "Ministerio de Ciencia y Tecnologia" and Catalan Autonomous Government (projects BQU2002-04587-C02-02 and 2001SGR-0044, respectively). The stay in Barcelona of LC was supported by the EU through a TMR contract with CESCA/CEPBA.

[1] Part I: P. Wautelet, J. Le Moigne, V. Videva, P. Turek, *J. Org. Chem.* **2003**, *68*, 8025–8036.

[2] Part II: L. Catala, J. Le Moigne, N. Kyritsakas, P. Rey, J. J. Novoa, P. Turek, *Chem. Eur. J.* **2001**, *7*, 2466–2480.

[3] For recent general reviews on molecular magnetism, see a) *Magnetic Properties of Organic Materials* (Ed.: P. M. Lahti), Marcel Dekker, New York, **1999**; b) *Molecular Magnetism* (Eds.: K. Itoh, M. Kinoshita), Gordon and Breach, Kodansha, Tokyo, **2000**; c) π *-Electron magnetism: From molecules to magnetic materials*, *Vol. 100* (Ed.: J. Veciana), Springer, **2001**; d) *Magnetism: Molecules to Materials*, *Vol. I–IV* (Eds.: J. S. Miller and M. Drillon), Wiley-VCH, Weinheim, **2001–2003**; e) B. Pilawa, *Ann. Phys.* **1999**, *3*, 191–254; f) J. A. Crayston, J. N. Devine, J. C. Walton, *Tetrahedron* **2000**, *56*, 7829–7857.

[4] a) J. S. Miller, *Adv. Mater.* **1992**, *4*, 298–300; b) J. S. Miller, *Adv. Mater.* **1992**, *4*, 435–484; c) A. J. Epstein, *MRS Bull.* **2003**, *28*, 492–498.

[5] a) A. Caneschi, D. Gatteschi, R. Sessoli, P. Rey, *Acc. Chem. Res.* **1989**, *22*, 392–398; b) H. O. Stumpf, L. Ouahab, Y. Pei, D. Grandjean, O. Kahn, *Science* **1993**, *261*, 447–449; c) K. Inoue, T. Hayamizu, H. Iwamura, D. Hashizume, Y. Ohashi, *J. Am. Chem. Soc.* **1996**, *118*, 1803–1804.

[6] a) J. Cirujeda, E. Hernàndez-Gasio, C. Rovira, J.-L. Stanger, P. Turek, J. Veciana, *J. Mater. Chem.* **1995**, *5*, 243–252; b) M. Matsuchida, A. Izuoka, T. Sugawara, T. Kobayashi, N. Wada, N. Takeda, M. Ishikawa, *J. Am. Chem. Soc.* **1997**, *119*, 4369–4379; c) F. M. Romero, R. Ziessel, M. Bonnet, Y. Pontillon, E. Ressouche, J. Schweizer, B. Delley, A. Grand, C. Paulsen, *J. Am. Chem. Soc.* **2000**, *122*, 1298–1309.

[7] a) M. Deumal, J. Cirujeda, J. Veciana, M. Kinoshita, Y. Hosokoshi, J. J. Novoa, *Chem. Phys. Lett.* **1997**, *265*, 190–199; b) M. Deumal, J. Cirujeda, J. Veciana, J. J. Novoa, *Adv. Mater.* **1998**, *10*, 1461–1466; c) M. Deumal, J. Cirujeda, J. Veciana, J. J. Novoa, *Chem. Eur. J.* **1999**, *5*, 1631–1642; d) M. Deumal, M. A. Robb, J. J. Novoa, *Polyhedron* **2003**, *22*, 1935–1944.

[8] a) K. Itoh, *Pure Appl. Chem.* **1978**, *50*, 1251–1259; b) H. Iwamura, *Pure Appl. Chem.* **1986**, *58*, 187–196; c) H. Iwamura, *Pure Appl. Chem.* **1987**, *59*, 1595–1604; d) H. Iwamura, *Pure Appl. Chem.* **1993**, *65*, 57–64; e) H. Iwamura, *Adv. Phys. Org. Chem.* **1990**, *26*, 179–253; f) D. A. Dougherty, *Acc. Chem. Res.* **1991**, *24*, 88–94; g) H. Iwamura, N. Koga, *Acc. Chem. Res.* **1993**, *26*, 346–351; h) A. Rajca, *Chem. Rev.* **1994**, *94*, 871–893; i) K. Itoh, Y. Sawaki, A. Izuoka, T. Sugawara, F. Miko, H. Iwamura, *J. Am. Chem. Soc.* **1990**, *112*, 4074–4075; j) A. Rajca, J. Wongsriratanakul, S. Rajca, *Science* **2001**, *294*, 1503–1505.

[9] a) H. Nishide, *Adv. Mater.* **1995**, *7*, 937–941; b) H. Nishide, T. Ozawa, M. Miyasaka, E. Tsuchida, *J. Am. Chem. Soc.* **2001**, *123*, 5942–5946; c) M. Miyasaka, Y. Saito, H. Nishide, *Adv. Funct. Mater.* **2003**, *13*, 113–117.

[10] a) H. C. Longuet-Higgins, *J. Chem. Phys.* **1950**, *18*, 265–274; b) N. Mataga, *Theor. Chim. Acta* **1968**, *10*, 372–376; c) W. T. Borden, E. R. Davidson, *J. Am. Chem. Soc.* **1977**, *99*, 4587–4594; d) A. A. Ovchinnikov, *Theor. Chim. Acta* **1978**, *47*, 297–304; e) W. T. Borden, H. Iwamura, J. A. Berson, *Acc. Chem. Res.* **1994**, *27*, 109–116.

[11] Recent reports: a) D. A. Shultz, A. K. Boal, G. T. Farmer, *J. Org. Chem.* **1998**, *63*, 9462–9469; b) R. M. Fico, M. F. Hay, S. Reese, S. Hammond, E. Lambert, M. A. Fox, *J. Org. Chem.* **1999**, *64*, 9386–9392; c) W. Adam, M. Baumgarten, W. Maas, *J. Am. Chem. Soc.* **2000**, *122*, 6735–6738; d) V. M. Domingo, C. Aleman, E. Brillas, L. Juliá, *J. Org. Chem.* **2001**, *66*, 4058–4061; e) D. A. Shultz, S. H. Bodnar, H. Lee, J. W. Kampf, C. D. Incarvito, A. L. Rheingold, *J. Am. Chem. Soc.* **2002**, *124*, 10054–10061; f) A. Dei, D. Gatteschi, C. Sangregorio, L. Sorace, M. G. F. Vaz, *Inorg. Chem.* **2003**, *42*, 1701–1706.

[12] a) M. Dvolaitzky, R. Chiarelli, A. Rassat, *Angew. Chem.* **1992**, *104*, 180–181; *Angew. Chem. Int. Ed. Engl.* **1992**, *31*, 180–181; b) F. Kanno, K. Inoue, N. Koga, H. Iwamura *J. Am. Chem. Soc.* **1993**, *115*, 847–850; c) S. K. Silverman, D. Dougherty, *J. Phys. Chem.* **1993**, *97*, 13273–13283; d) N. Yoshioka, P. M. Lahti, K. Takashi, Y. Kuzumaki, E. Tsuchida, H. Nishide, *J. Org. Chem.* **1994**, *59*, 4272–4280; e) S. Fang, M. S. Lee, D. A. Hrovat, W. T. Borden, *J. Am. Chem. Soc.* **1995**, *117*, 6727–6731; f) J. Fujita, M. Tanka, H. Suemune, N. Koga, K. Matsuda, H. Iwamura, *J. Am. Chem. Soc.* **1996**,

118, 9347–9351; g) D. Schultz, A. K. Boal, G. T. Farmer, *J. Am. Chem. Soc.* **1997**, *119*, 3846–3847.
[13] a) A. Rajca, S. Rajca, *J. Am. Chem. Soc.* **1996**, *118*, 8121–8126; b) A. Rajca, J. Wongsriratanakul, S. Rajca, *J. Am. Chem. Soc.* **1997**, *119*, 11674–11686; c) A. Rajca, J. Wongsriratanakul, S. Rajca, R. Cerny, *Angew. Chem.* **1998**, *110*, 1284–1288; *Angew. Chem. Int. Ed.* **1998**, *37*, 1229–1232.
[14] L. Catala, P. Turek, J. Le Moigne, A. De Cian, N. Kyritsakas, *Tetrahedron Lett.* **2000**, *41*, 1015–1018.
[15] F. M. Romero, R. Ziessel, A. De Cian, J. Fischer, P. Turek, *New J. Chem.* **1996**, *20*, 919–924.
[16] M. Alami, F. Ferri, G. Linstrumelle, *Tetrahedron Lett.* **1993**, *34*, 6403–6406.
[17] E. F. Ullman, J. H. Osiecki, D. G. B. Boocock, R. Darcy, *J. Am. Chem. Soc.* **1972**, *94*, 7049–7059.
[18] N. Miyaura, A. Suzuki, *Chem. Rev.* **1995**, *95*, 2457–2483.
[19] Z. Z. Zhong, H. N. C. Wong, *J. Org. Chem.* **1994**, *59*, 33–41.
[20] G. Ulrich, R. Ziessel, *Tetrahedron Lett.* **1994**, *35*, 1215–1218.
[21] J. E. Wertz, J. R. Bolton, *Electron Spin Resonance, Elementary Theory and Practical Applications*, Chapman and Hall **1994**, p. 112.
[22] WINEPR Simfonia software, Bruker Analytische Messtechnik GmbH, **1995–1996**, Version 1.25.
[23] a) D. A. Shultz, R. M. Fico, Jr., S. H. Bodnar, R. K. Kumar, K. E. Vostrikova, J. W. Kampf, P. D. Boyle, *J. Am. Chem. Soc.* **2003**, *125*, 11761–11771; b) D. A. Shultz, R. M. Fico, Jr., H. Lee, J. W. Kampf, K. Kirschbaum, A. A. Pinkerton, P. D. Boyle, *J. Am. Chem. Soc.* **2003**, *125*, 15426–15432.
[24] a) K. Yoshizawa, A. Chano, A. Ito, K. Tanaka, T. Yamabe, H. Fujita, J. Yamauchi, M. Shiro, *J. Am. Chem. Soc.* **1992**, *114*, 5994–5998; b) Y. Teki, T. Takui, K. Itoh, H. Iwamura, K. Kobayashi, *J. Am. Chem. Soc.* **1986**, *108*, 2147–2156.
[25] a) J. A. Berson, in *The Chemistry of Quinonoid Compounds*, *Vol. 11* (Eds.: S. Patai and Z. Rappoport), **1988**, pp. 481; b) K. Matsuda, H. Iwamura, *J. Chem. Soc. Perkin Trans. 2* **1998**, 1023–1026.
[26] a) M. Tanaka, K. Matsuda, T. Itoh, H. Iwamura, *J. Am. Chem. Soc.* **1998**, *120*, 7168–7173; b) P. M. Lahti, Y. Liao, M. Julier, F. Palacio, *Synth. Met.* **2001**, *122*, 485–493.
[27] a) E. Belorizky, *J. Phys. I* **1993**, *3*, 423–445; b) E. Belorizky, P. H. Fries, *J. Chim. Phys. Phys.-Chim. Biol.* **1993**, *90*, 1077–1100; c) E. Belorizky, M. Jeannin, P. Rey, A. Rassat, *Solid State Commun.* **1993**, *85–88*, 735–737.
[28] A. Rajca, S. Rajca, *J. Am. Chem. Soc.* **1995**, *117*, 806–816.
[29] a) S. Murata, H. Iwamura, *J. Am. Chem. Soc.* **1991**, *113*, 5547–5556; b) T. Mitsumori, K. Inoue, N. Koga, H. Iwamura, *J. Am. Chem. Soc.* **1995**, *117*, 2467–2478.
[30] H. M. McConnell, *J. Chem. Phys.* **1963**, *39*, 1910.
[31] F. H. Allen, *Acta Crystallogr. Sect. B* **2002**, *58*, 380–388.
[32] J. A. Wytko, J. Weiss, *Tetrahedron Lett.* **1991**, *32*, 7261–7264.
[33] M. Lamchen, T. W. Mittag, *J. Chem. Soc.* **1966**, 2300–2303.
[34] B3LYP is a density functional obtained by taking the three parameter non-local exchange functional of Becke and the non-local correlation functional of Lee–Yang–Parr a) A. D. Becke, *J. Chem. Phys.* **1993**, *98*, 5648–5652; b) C. Lee, W. Yang, R. G. Parr, *Phys. Rev. B* **1988**, *37*, 785–789.
[35] R. Parr, W. Yang, *Density Functional Theory of Atoms and Molecules*, Oxford University Press, New York, **1989**.
[36] J. S. Binkley, J. A. Pople, W. J. Hehre, *J. Am. Chem. Soc.* **1980**, *102*, 939–947.
[37] Gaussian 98 (Revision A.7), M. J. Frisch, G. W. Trucks, H. B. Schlegel, G. E. Scuseria, M. A. Robb, J. R. Cheeseman, V. G. Zakrzewski, J. A. Montgomery, R. E. Stratmann, J. C. Burant, S. Dapprich, J. M. Millam, A. D. Daniels, K. N. Kudin, M. C. Strain, O. Farkas, J. Tomasi, V. Barone, M. Cossi, R. Cammi, B. Mennucci, C. Pomelli, C. Adamo, S. Clifford, J. Ochterski, G. A. Petersson, P. Y. Ayala, Q. Cui, K. Morokuma, D. K. Malick, A. D. Rabuck, K. Raghavachari, J. B. Foresman, J. Cioslowski, J. V. Ortiz, B. B. Stefanov, G. Liu, A. Liashenko, P. Piskorz, I. Komaromi, R. Gomperts, R. L. Martin, D. J. Fox, T. Keith, M. A. Al-Laham, C. Y. Peng, A. Nanayakkara, C. Gonzalez, M. Challacombe, P. M. W. Gill, B. G. Johnson, W. Chen, M. W. Wong, J. L. Andres, M. Head-Gordon, E. S. Replogle, J. A. Pople, Gaussian, Inc., Pittsburgh, PA, **1998**.

Received: June 3, 2004
Revised: September 7, 2004
Published online: January 26, 2005